SCIENTIFIC REPORTS

OPEN

SUBJECT AREAS:
BIOTECHNOLOGY
IMAGING
APPLIED PHYSICS
FLUORESCENCE IMAGING

Received
11 September 2012

Accepted
1 October 2012

Published
12 November 2012

Correspondence and requests for materials should be addressed to P.A.V. (Pablo.A.Valdes@Dartmouth.edu) or D.W.R. (David.W.Roberts@Dartmouth.edu)

Quantitative, spectrally-resolved intraoperative fluorescence imaging

Pablo A. Valdés[1,2,3], Frederic Leblond[1], Valerie L. Jacobs[2], Brian C. Wilson[5], Keith D. Paulsen[1,2,4] & David W. Roberts[2,3,4]

[1]Thayer School of Engineering, Dartmouth College, Hanover, NH 03755, USA, [2]Dartmouth Medical School, Dartmouth College, Hanover, NH 03755, USA, [3]Section of Neurosurgery, Dartmouth Hitchcock Medical Center, Lebanon, New Hampshire 03756, USA, [4]Norris Cotton Cancer Center, Dartmouth Hitchcock Medical Center, Lebanon, New Hampshire 03756, USA, [5]University of Toronto, Ontario Cancer Institute, 610 University Avenue, Toronto, Ontario M5G 2M9, Canada.

Intraoperative visual fluorescence imaging (vFI) has emerged as a promising aid to surgical guidance, but does not fully exploit the potential of the fluorescent agents that are currently available. Here, we introduce a quantitative fluorescence imaging (qFI) approach that converts spectrally-resolved data into images of absolute fluorophore concentration pixel-by-pixel across the surgical field of view (FOV). The resulting estimates are linear, accurate, and precise relative to true values, and spectral decomposition of multiple fluorophores is also achieved. Experiments with protoporphyrin IX in a glioma rodent model demonstrate *in vivo* quantitative and spectrally-resolved fluorescence imaging of infiltrating tumor margins for the first time. Moreover, we present images from human surgery which detect residual tumor not evident with state-of-the-art vFI. The wide-field qFI technique has broad implications for intraoperative surgical guidance because it provides near real-time quantitative assessment of multiple fluorescent biomarkers across the operative field.

The clinical foundation of surgical oncology is underpinned by the simple but universal premise that for most solid tumors achieving complete resection improves patient outcomes. Unfortunately, despite significant advances in surgical technology and technique[1–4], rates of complete resection remain surprisingly low and/or the need for re-excision persists in many primary cancers (e.g., in brain[5,6], breast[7], and prostate[8], among others). Intraoperative tissue characterization also enables conservation of normal tissue, which is critical to functional preservation or patient satisfaction and quality of life. For example, re-excision rates in breast lumpectomy have been reported to be as high as 40% in some studies[9], largely because of residual disease found at the margin of the resected specimen that was not apparent to the surgeon at time of procedure. Glandular preservation in prostate cancer surgery is desirable clinically[10], but has not been widely adopted because surgical margins have been difficult to identify intraoperatively without histologically assessing the excised tissue in the operating room (OR)[11].

Nowhere are the principles of complete resection and the application of technology to meet the concomitant procedural challenges more evident than in neurosurgical oncology, where the highly invasive and infiltrative nature of malignant glioma typically leads to recurrence[12,13]. Major technologies and procedural trends that apply across surgical specialties (i.e., wide-field, white-light visualization of the surgical field through the operating microscope (OM)[14], navigational tracking[15], image-guidance[16], intraoperative imaging[17], etc.) were born in neurosurgery ORs, which have become a clinical platform for technology innovation and translation across all of surgery.

The most recent advances, now found in many modern OMs, involve use of light at specific wavelength(s) which stimulates fluorescent emissions from biomarkers that can be associated with specific tissues in the field-of-view (FOV), and offer the hope of identifying disease, intraoperatively, at the cellular and/or molecular levels[2,18–20]. Accordingly, visualization of protoporphyrin IX (PpIX) red fluorescence induced by oral administration of 5-aminolevulinic acid (ALA) has become standard-of-care for resection of high-grade glioma in Germany based on outcomes from a randomized multi-center Phase III trial comparing progression free survival in patients undergoing either fluorescence-guided resection or conventional resection under white light visualization[18].

While these OMs have allowed surgeons wide-spread access to visual fluorescence imaging (vFI) in the OR, the information is *not quantitative* and resection decisions have been reached based on *subjective assessments of the visible fluorescence* (e.g., red fluorescence from PpIX) from the surgical surface. Current intraoperative vFI does not correct for the distorting, non-linear effects of tissue optical properties[21] which reduces the correlation

Table 1 | Phantom optical properties at λ_x = 405 nm and λ_m = 635 nm

	$\mu_{a,x}(cm^{-1})$	$\mu'_{s,x}(cm^{-1})$	$\mu_{a,m}(cm^{-1})$	$\mu'_{s,m}(cm^{-1})$
△	20	15	0.02	8.7
□	20	20	0.04	11.6
○	20	25	0.06	14.5
▲	40	15	0.02	8.7
■	40	20	0.04	11.6
●	40	25	0.06	14.5
▲	60	15	0.02	8.7
■	60	20	0.04	11.6
●	60	25	0.06	14.5

Optical absorption (μ_a) and reduced scattering (μ'_s) phantom combinations. Symbol used to denote each case in **Fig 1** is shown.

between perceived fluorescence and actual biomarker concentration. Indeed, vFI leaves significant tumor undetected[22,23] – it does not take full advantage of the specificity of fluorescent biomarkers (e.g., because diagnostic concentrations exist which are not visible[22,23]), or their spectral signatures (e.g., because single bandpass or longpass filters have typically been used to collect the fluorescence signal[2,19]). Spectrally-resolved detection, i.e., detection of the full spectrum, enables decomposition of non-specific autofluorescence in tissue, which improves image contrast and detection accuracy of cancer-specific biomarkers[23,24]. With the advent of intraoperative fluorescence imaging and accompanying fluorophores for surgical guidance (e.g., PpIX[18], folate receptor targets[2], fluorescent peptides[3], blood pooling agents such as fluorescein and indocyanine green[19], etc.), decomposition of overlapping fluorescent agents from the same emission signal becomes possible with spectrally-resolved approaches, thus allowing simultaneous, spatially-coregistered *in vivo* imaging of multiple reporters[19,25].

In this paper, we present the first demonstration of wide-field quantitative fluorescence imaging (qFI) *in vivo* for intraoperative surgical guidance. Critical to this success is spectrally-resolved image capture with concomitant correction of the emitted fluorescence for tissue optical property variations and fast (near real-time) data processing to estimate absolute fluorophore concentrations pixel-by-pixel across the FOV. Quantitative results are reported for both animal and human intracranial tumors in the intraoperative setting. Here, we show pre-clinical imaging of PpIX and fluorescein in tissue, resulting from simultaneous detection of full visible spectrum fluorescence in the same animal tumors. Quantitative identification of more than one fluorophore within the same FOV offers new possibilities for simultaneously delineating multiple tissue characteristics of critical importance to the surgeon. We also show the first human results of qFI as a novel imaging technique to improve tumor detection during the resection of glioblastoma multiforme (GBM). While we present these results in the setting of neurosurgery, the data acquisition and processing methods reported for intraoperative wide-field qFI of absolute concentrations of multiple flourophores are readily applied to other fluorescent reporters and/or surgical oncology procedures.

Results

Phantom validation. *Quantification of fluorophore concentration.* The quantitative performance of our wide-field qFI instrumentation in terms of estimating fluorophore concentration was evaluated and validated in phantoms. A spectrally-constrained dual band normalization[26] was used to correct the raw fluorescence signal for the nonlinear distortions caused by tissue optical properties at both the excitation and fluorescence emission wavelengths (**Methods**). The approach compensates for varying optical attenuation in tissue which enables quantification of absolute fluorophore concentrations. Previously-validated, tissue-simulating liquid phantoms fabricated with varying optical absorption (μ_a) and reduced scattering (μ_s') properties at the excitation and main emission peak of PpIX (λ = 405 nm and λ = 635 nm, respectively) were formed with increasing PpIX concentrations from 0.02 to 5 μg/ml, commensurate with the range commonly found in normal and pathological tissues. **Table 1** summarizes the 9 combinations of absorption and scattering optical properties that were mixed with each of 9 concentrations of PpIX (total of 81 phantoms) **(Methods).**

We acquired spectrally-resolved, wide-field image data with our qFI system to calculate pixel-specific PpIX concentrations, C_{PpIX}, across the FOV (**Methods**) and compared these values to the actual PpIX concentrations shown in **Figure 1**. The linearity of the qFI estimate with increasing C_{PpIX} averaged over pixels for all 9 combinations of phantom optical properties resulted in a coefficient of determination, R^2 = 0.88. The mean percentage error (mPE) in the imaged C_{PpIX} estimates was 24% (PE range: 0.3 – 71.4%). The mean coefficient of variation (pixel standard deviation divided by pixel mean), mCOV, is also shown in **Figure 1** as a function of true C_{PpIX} for each optical phantom combination and indicates a mean of 2.7% with a range from 0.1% to less than 45% (at the lowest PpIX concentration of 0.02 μg/ml and highest optical absorption).

To relate these results to state-of-the-art vFI, we integrated the area under the curve of the raw fluorescence signal, F_{RAW}, over the range λ = 610−720 nm in **Figure 1**. In this case, not only is the linearity of the response to increasing C_{PpIX} significantly degraded (R^2 = 0.27 for C_{PpIX} > 0.30 μg/ml; R^2 < 0.1 for C_{PpIX} > 0.02 μg/ml), but the C_{PpIX} estimates are also less accurate (mPE = 55%) when the phantom optical properties were changed but C_{PpIX} remained the same.

Spectral decomposition of multiple fluorophores. We evaluated the ability of our qFI system to spectrally resolve multiple fluorophores by adding concentrations of fluorescein to the homogeneously distributed PpIX phantoms of increasing C_{PpIX}. **Figure 2** shows qFI estimates as a function of increasing (true) C_{PpIX} for 4 different concentrations of fluorescein. Here, we considered C_{PpIX} ranging from 0.156 μg/ml to 1.25 μg/ml combined with fluorescein concentrations from 1.25 to 10 μg/ml which are representative of clinically relevant concentrations[23]. The strongly linear and accurate relationship between wide-field qFI-derived C_{PpIX} estimates and the actual PpIX concentrations was preserved (R^2 = 0.99, mPE = 13%) across all FOVs and phantom concentrations (PE range: 0.5 and 56.3%). COV response is also shown in **Figure 2** and mCOV was 1.2% (mCOV range: 0.2 – 9.2%).

Animal studies. *In vivo* qFI was evaluated in an established rodent model of GBM, which displays the histopathological hallmarks of the disease, including invasion of parenchyma and periventricular spread with single cell infiltration. Animals implanted with CNS-1 tumors were given 100 mg/kg of ALA 2 hrs prior to surgery. At the start of surgery, four (4) of these animals also received an i.v. injection of 100 mg/kg of 10% fluorescein sodium solution. Exogenous ALA administration leads to selective accumulation of PpIX in tumors whereas fluorescein functions as a blood pooling agent, preferentially accumulating in regions of leaky tumor vasculature.

Quantification of fluorophore concentration. In 4 of the animals receiving only ALA, we compared wide-field qFI estimates of C_{PpIX} with *in vivo* spectroscopy probe recordings in both tumor and normal brain in multiple locations in each animal (for a total of n = 41 samples). In previous work[27], the accuracy of the probe was evaluated in detail and the instrument was found to reproduce known phantom and *in vivo* values of C_{PpIX} with an error of less than 10%. Here, we considered the probe readings to represent the gold standard for C_{PpIX}. In paired t-tests, no statistically significant differences were found between the two data sets. **Supplementary Figure 2** presents a

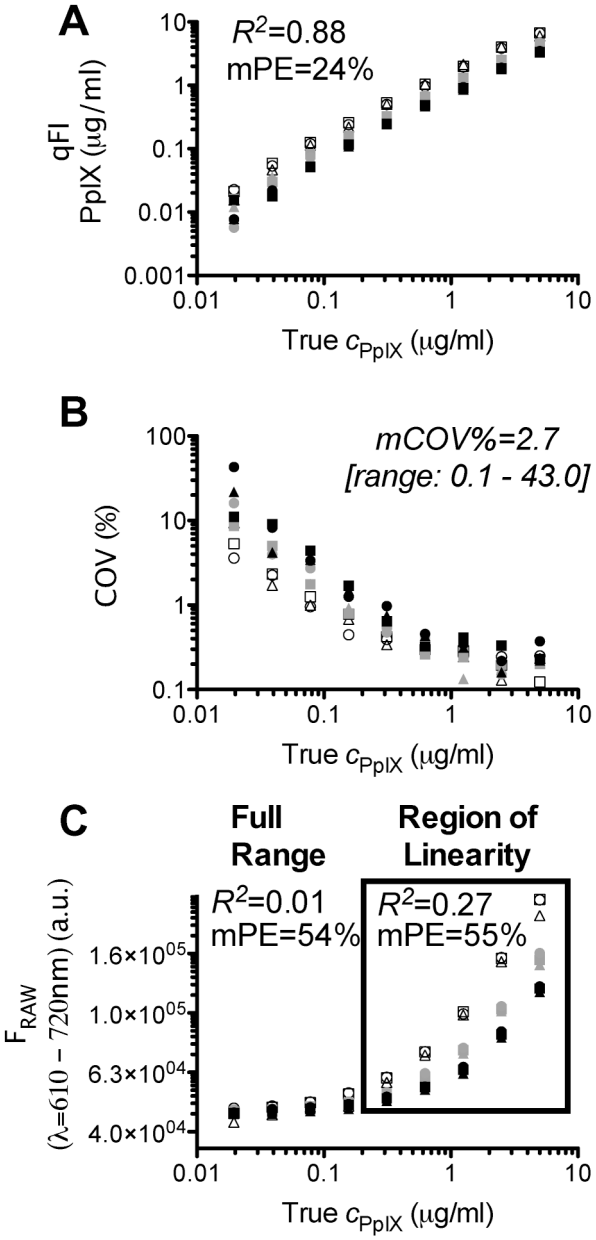

Figure 1 | Wide-field image estimate versus true PpIX concentration, C_{PpIX}, in phantoms with different absorption and scattering optical properties (see Table 1). (A) Pixel-averaged qFI estimates of C_{PpIX}. (B) Coefficient of variation, COV, across the FOV. (C) Area under the raw optical signal (fluorescence intensity) curve from 610–720 nm. R^2 = coefficient of determination; mPE = mean percentage error; mCOV = mean coefficient of variation.

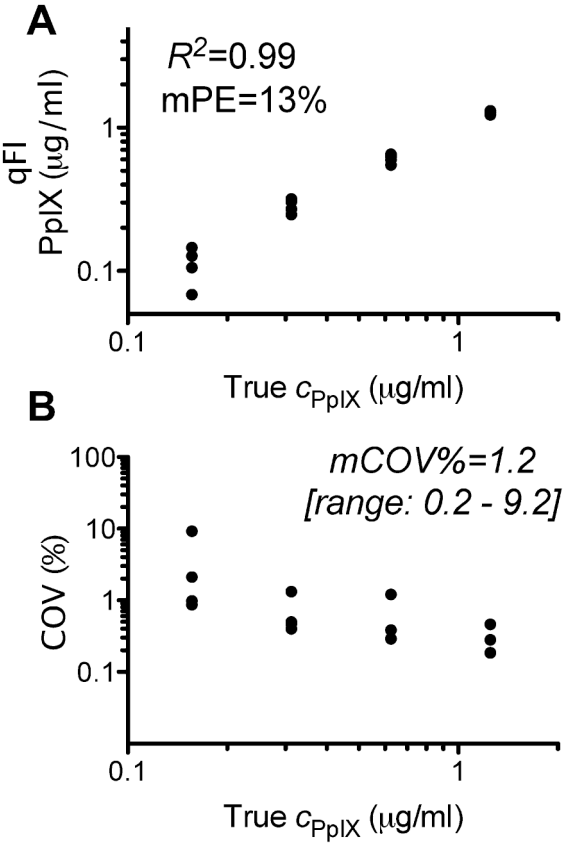

Figure 2 | Wide-field image estimate versus changing PpIX concentration, C_{PpIX}, in phantoms with different fluorescein concentrations (10, 5, 2.5, 1.25 μg/ml). (A) Pixel-averaged qFI estimates of C_{PpIX}. (B) Coefficient of variation, COV, across the FOV. Multiple points per C_{PpIX} represent different fluorescein concentrations.

scatter plot of C_{PpIX} estimates from the wide-field qFI image locations coregistered with the position of the probe against the probe values. A linear relationship is evident with a statistically-significant ($p < 0.0001$) correlation coefficient of $R = 0.79$. When probe C_{PpIX} was greater than 40 ng/ml, mPE for the qFI estimates of C_{PpIX} was less than 35%.

Figure 3 shows a representative set of images from a typical animal in the ALA-only group which illustrates white-light, vFI, qFI and qFI+white-light views of the same surgical field. A red PpIX fluorescence is observed in the tumor bulk under vFI. Congruence between the vFI and white-light indications of tumor is evident. Corresponding qFI maps of PpIX concentrations of the same FOV reveal $C_{PpIX} > 150$ ng/ml in the tumor bulk. Interestingly, infiltrating tumor margins ($C_{PpIX} \sim 100$ ng/ml) outside the tumor bulk are evident on qFI, but not vFI (**Fig. 3c**, white arrow), demonstrating improved margin delineation with qFI at PpIX concentrations which were below the visual threshold for detection.

Spectral decomposition of multiple fluorophores. Four (4) animals receiving doses of both ALA and fluorescein were imaged after surgical exposure of the tumor to evaluate the spectral separation of the contributions of these two fluorophores. **Figure 4** shows representative results from a typical animal where white-light, vFI and qFI views of the same surgical field are displayed. The vFI presentation in the bulk tumor is visually dominated by the green fluorescein color. The wide-field C_{PpIX} image and the normalized fluorescein map indicate localization of both molecules with greatest concentrations in similar regions of the tumor bulk, but with some distributed heterogeneity (including in the immediately adjacent and surrounding margin). Again, qFI detected significant levels of PpIX in the infiltration zone which would have otherwise gone undetected with vFI (see arrows in **Fig. 4C** vs. **Fig 4B**). Sample spectra are also shown which illustrate the decomposition of the relative contributions of each fluorophore (and tissue autofluorescence) despite the lack of visual discrimination.

Human studies. To date, surgical fields in 12 brain tumor patients receiving 20 mg/kg of ALA approximately 3 hours prior to the procedure have been assessed with the qFI system. **Figure 5** shows a comparison of vFI and qFI in a representative case. At the start of this surgery, vFI indicates a heterogeneous distribution of PpIX fluorescence whereas the corresponding qFI view demonstrates the

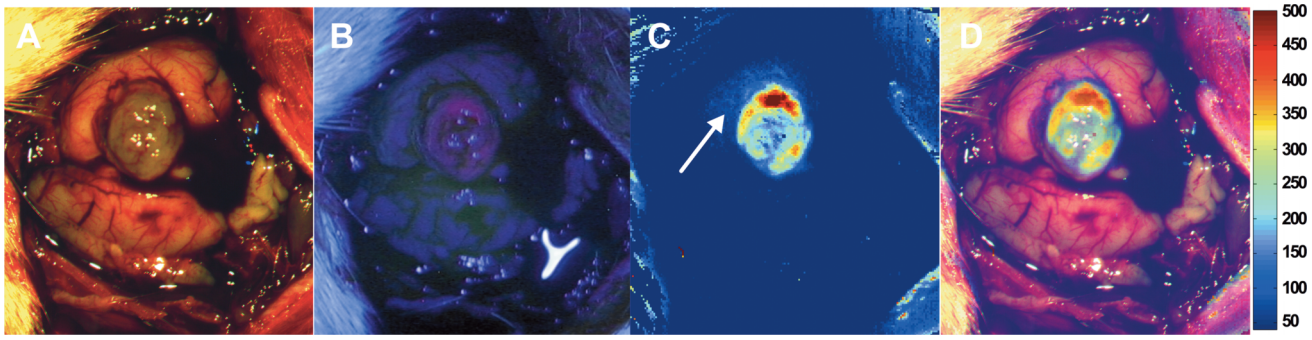

Figure 3 | Wide-field qFI estimates of C_{PpIX} in a rodent model of glioma. (A) White light FOV. (B) Corresponding vFI demonstrating red PpIX fluorescence in the tumor bulk. (C) Map of qFI estimates of C_{PpIX}. (D) Corresponding image overlay demonstrating C_{PpIX} >150 ng/ml in the tumor bulk, as well as significant (C_{PpIX} ~100 ng/ml) PpIX in the infiltrating margin (white arrow). Color bar values are in ng/ml.

presence of more significant, previously undetected tumor biomarker. Normal brain similarly does not show spectral evidence of tumor based on the qFI view which was confirmed by probe measurement. A similar series of image acquisitions near the end of surgery in the same patient illustrates no evidence of disease in the vFI view but histologically-confirmed residual tumor in the qFI images. Corresponding spectra from histologically-confirmed tumor-positive (near the end of surgery) and tumor-negative portions (at the end of surgery) of the qFI-derived C_{PpIX} map are shown which demonstrate the presence and absence of PpIX signal, respectively (**Fig. 5L**).

Discussion

In this paper, we describe the implementation and evaluation of a fast (near real-time), quantitative and spectrally-resolved wide-field fluorescence imaging approach for intraoperative identification and delineation of tumor during surgery. Critical to the success of the technique is acquisition of white-light reflectance spectra to correct the detected fluorescence for attenuation caused by tissue optical absorption and scattering in the fluorescence excitation and emission wavelength bands. The method produces quantitative estimates of fluorophore concentration, but also enables spectral decomposition of contributions from multiple fluorophores in the FOV.

Phantom results demonstrate the sensitivity and linearity of the approach to PpIX fluorescence. Specifically, we detected PpIX concentrations as low as 20 ng/ml, independently of phantom optical properties, with linear changes in the imaged signal to increases in the true PpIX concentration up to 5000 ng/ml. The absolute accuracy in the wide-field C_{PpIX} image estimates was better than 25% and their precision resulted in a coefficient of variation across the image of less than 10% for all optical property combinations provided C_{PpIX} was greater than 40 ng/ml. Our *in vivo* human data indicate that a detection threshold of ~100 ng/ml will provide positive predictive values in excess of 90%[22,23]. Importantly, qFI was at least an order of magnitude more sensitive to PpIX concentration than vFI (~40 ng/ml vs. ~600 ng/ml), and generated improved contrast (~10:1) at concentrations at least one order of magnitude lower (~40 ng/ml vs. ~600 ng/ml for qFI compared to vFI, respectively).

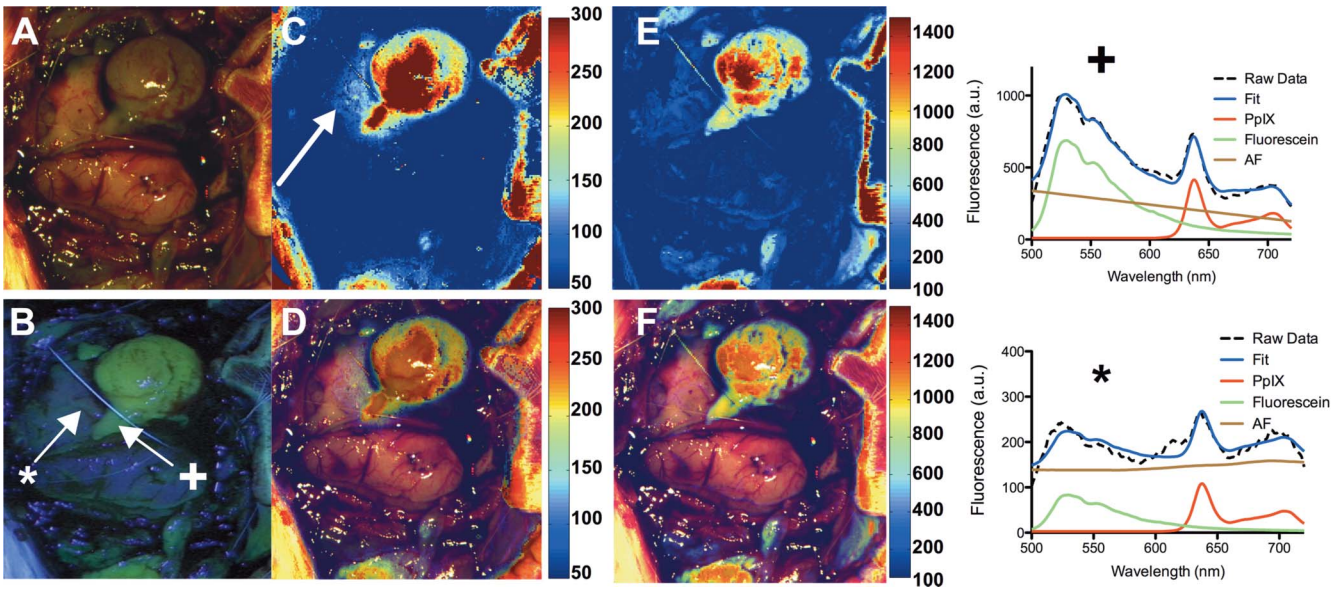

Figure 4 | Wide-field qFI in the presence of two fluorophores in a rodent model of glioma. (A) White light FOV. (B) Corresponding vFI demonstrates green fluorescein fluorescence in the tumor bulk, and no visible PpIX red fluorescence. (C) Map of qFI estimates of C_{PpIX}. (D) Corresponding image overlay shows C_{PpIX} >200 ng/ml in the tumor bulk. (E) Map of normalized fluorescein levels. (F) Corresponding image overlay demonstrates fluorescein levels in the tumor bulk as well as diffusely scattered through normal brain. Significant PpIX concentration (C_{PpIX} ~100 ng/ml) was found in the infiltrating margin (white arrow in C) with minimal fluorescein present. Spectral decomposition (far right) indicates the varying contributions (at arrow locations in B marked +, top spectral plot, and *, bottom spectral plot) from each fluorophore in the FOV. Color bar values for C and D are in ng/ml and for E and F in normalized arbitrary units.

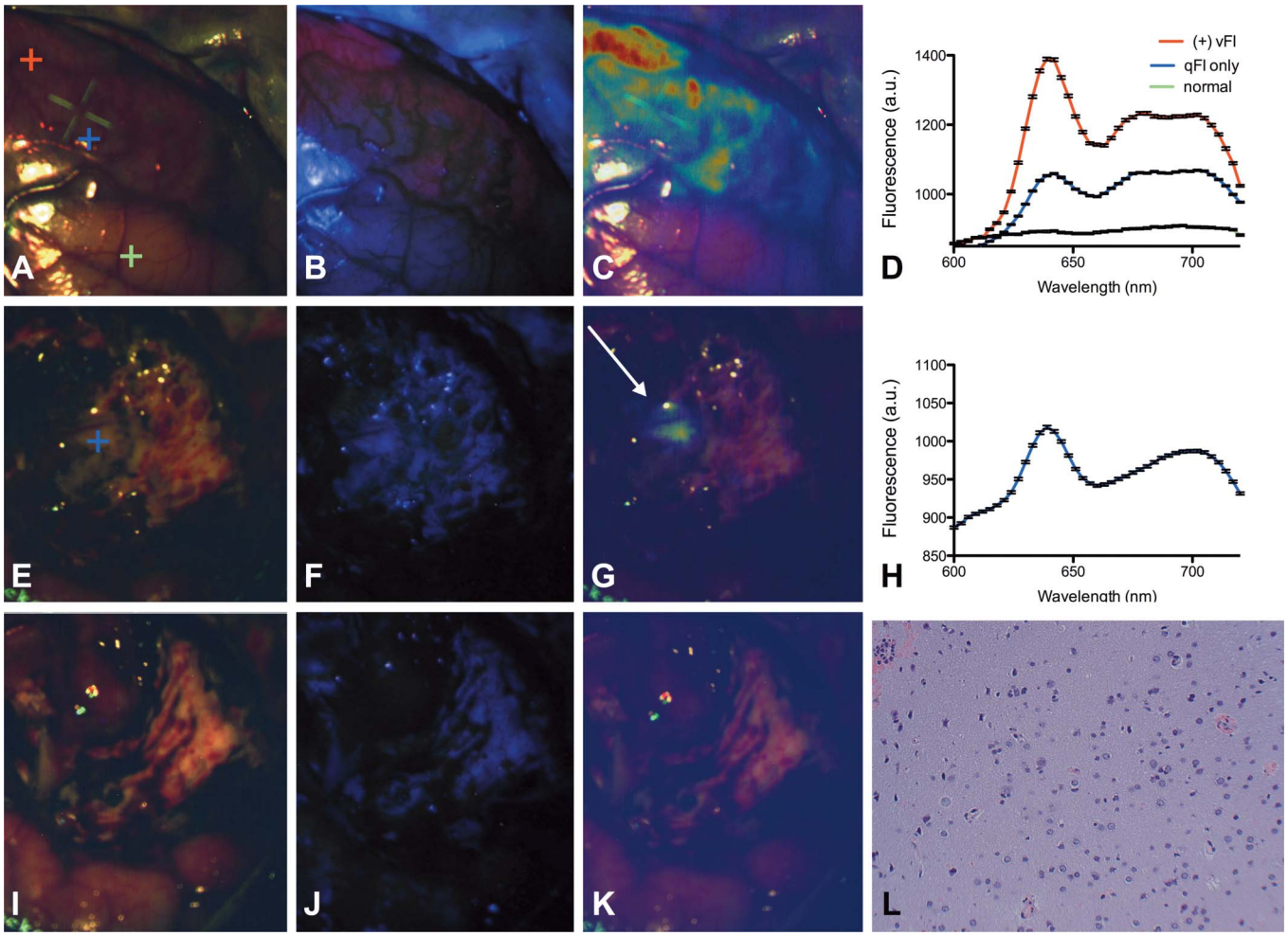

Figure 5 | Wide-field qFI during a human GBM surgery. Images at the beginning (A–C), near the end (E–G), and at the end of the case (I–K) show vFI, white light, and white light+qFI views, respectively. High levels of PpIX are evident at the start of surgery (in B), whereas near the end of surgery, no PpIX is noted on vFI (in F), but significant PpIX was found in qFI near the center of the FOV (in G) with histological corroboration as tumor (in L). At the end of surgery, no significant PpIX levels remained in the qFI acquisition (in K). Spectra obtained at the beginning of surgery (in D) from three locations (1 = vFI positive tumor, red mark in A; 2= qFI positive/vFI negative tumor, blue mark in A; 3 = normal brain, green mark in A), and spectrum acquired near the end of surgery (in H) from one location (1 = qFI positive/vFI negative tumor, blue mark in E) are shown.

Pre-clinical results in a rodent glioma model indicated that the qFI-derived C_{PpIX} was also linear with the response of our quantitative, direct-contact optical spectroscopy probe and yielded a highly statistically significant ($P < 0.001$) correlation coefficient of 0.79 based on 41 measurements obtained from multiple animals. When C_{PpIX} measured with the probe was greater than 40 ng/ml, the mean percentage error (assuming the probe is the gold standard) in the *in-vivo* qFI-derived C_{PpIX} estimates was 30% whereas the errors exceeded 100% when all probe data were included. These results are specific to this tumor biomarker and suggest that the *in-vivo* sensitivity of the qFI technique is presently about 40 ng/ml which is below the intraoperative threshold of 100 ng/ml based on our clinical experience with PpIX to date[22,23]. In these animals, we observed significant heterogeneity in the tumor bulk (with values ranging from 50 ng/ml to 500 ng/ml), and C_{PpIX} levels up to 100 ng/ml in the infiltrating margins that were not visibly apparent with vFI. These data indicate that our qFI technique can not only detect the more infiltrating margins of tumor, but also yields absolute concentrations with reasonable accuracy.

The importance of qFI relative to state-of-the-art vFI was particularly evident, and equally convincing, in the animals receiving both ALA and fluorescein as shown in **Figure 4** where the vFI view is substantially altered by the presence of fluorescein. Again, substantial PpIX concentration ($C_{PpIX} > 200$ ng/ml) is recovered in the tumor bulk that was not visually evident, and weaker but still accurate, PpIX concentrations ($C_{PpIX} \sim 100$ ng/ml) are found in the infiltrating tumor margins, providing evidence of improved detection of invasive disease. An important caveat to these results is that the fluorescein images are not quantitative (rather normalized) because we did not determine the qFI calibration factors or investigate the optimal excitation/emission normalization bands to correct for tissue optical property distortions of the fluorescein fluorescence signal. While this optimization and calibration can be done, the non-quantitative nature of the fluorescein images does not diminish the significance of the PpIX results nor the ability to decompose measured spectra into estimates of absolute concentrations of multiple fluorophores. Quantitative, multiple reporter imaging opens the door to novel fluorescence detection approaches in the intraoperative setting (e.g., measurement of reporter kinetics[28]).

The human data near the end of surgical resection was even more compelling in terms of the clinical importance of wide-field qFI surveillance. When tumor appeared to be completely removed by vFI, previously unidentified infiltrative tumor was evident with qFI enabling further resection (see **Figure 5**). In addition, wide-field qFI provided efficient detection compared with impractical, point-by-point application of a quantitative probe. These results suggest

improved infiltrative tumor margin detection will be possible with our quantitative qFI technique.

While the qFI results presented in this paper are impressive (particularly the data in phantoms where the true C_{PpIX} values are known and can be accurately quantified), further advances are likely to improve the wide-field qFI accuracy, *especially in vivo at concentrations below 40 ng/ml*. For example, better instrumentation fidelity (a more sensitive camera and powerful light source) should increase the accuracy of the technique. Further, the approach described here relies on normalization with respect to pre-selected excitation and fluorescence emission wavelength bands which have been optimized to correct for the attenuation effects of tissue optical properties. A model-based strategy that compensates the fluorescence signal by explicitly estimating tissue optical absorption and scattering across the full spectrum, is anticipated to be more accurate and reduce dependencies on instrumentation and measurement calibration/scaling factors to convert the raw signal acquisitions into concentration estimates[21,27]. Based on our experience during the development of the quantitative optical probe (which applies full-spectrum analyses), *in vivo* errors below 20% appear possible, although at the expense of considerably more computational effort that may be difficult to execute in near real-time in the OR.

In conclusion, we present a novel wide-field imaging technique, qFI, which provides quantitative and spectrally resolved images of fluorophore concentrations in (residual tumor) tissue, and readily integrates into the surgical workflow. Our approach demonstrates improved detection of residual disease compared to state-of-the-art vFI that could increase the completeness of tumor resection with preservation of normal function, which is known to correlate with improved patient outcomes. This method has potential for broad impact across other surgical oncology applications and in the detection of other fluorescent biomarkers of disease, including those that may be present simultaneously.

Methods

Quantitative fluorescence imaging (qFI) system design. The quantitative fluorescence imaging (qFI) system used in this study (dimensions = 22.0 cm x 5.0 cm x 8.5 cm, weight = 900 g) consisted of three main components: a custom optical adapter, a liquid crystal tunable filter (LCTF) (Cambridge Research Instruments), and a charged-coupled device (CCD) camera (PCO.Pixelfly, Cooke Corp.) connected to a computer control system as shown schematically and physically in **Supplementary Figure 1**. The custom adapter attached these components (LCTF and camera) to an optical port on a Zeiss Pentero OM, whereas commercially available components and optics (Edmund Optics) connected the LCTF and CCD camera. The LCTF performed fast (50 ms) single-band filtering (7 nm full-width at half-maximum) of incoming light in the visible range, λ = 400 – 720 nm, and displayed a wavelength specific response with a maximum transmittance of 64% at 710 nm. The CCD camera (1396 x 1024 pixels; 2 x 2 binning; 62% quantum efficiency at 580 nm) sensed incoming light and transmitted the digital data to a computer control system. It had an enhanced red-near-infrared mode which improved sensitivity in that spectral region. Custom LabView® software (National Instruments, Austin, TX) integrated control of the data acquisition, processing, and image display.

The surgeon's FOV through the OM was co-registered with the qFI data, providing one-to-one comparisons. At standard working distances between the OM and surgical field, the maximum and minimum FOVs were 50 mm x 40 mm and 10 mm x 7.5 mm, respectively. Spectrally-resolved acquisition ranged from 2 to 8 seconds per white light and fluorescence image capture. Here, we operated in the visible portion of the spectrum to image two clinically-approved fluorescent dyes (i.e., PpIX and fluorescein). With the advent of imaging agents in the near infrared (NIR)[25,29], the design could accommodate either an LCTF operating in the NIR or a dual visible-NIR LCTF.

Spectrally-resolved quantitative fluorescence imaging data. Each qFI acquisition captured a 3D image cube at 5 nm spectral resolution (for λ = 450 – 720 nm) under white light exposure followed by a 3D image cube at 3 nm spectral resolution (e.g., for λ = 600 – 720 nm for PpIX or 500 – 720 nm for PpIX plus fluorescein) during violet-blue light exposure. Wavelength range selection was electronic and depended on the wavelength region of interest so as to cover the main spectral features of each imaging agent.

A 3D image cube (x, y, λ) was stored as a series of 2D spatial images (x, y) at a specific wavelength (λ). Each individual pixel's spatial coordinate (x, y) corresponded to a location in the surgical field. We reconstructed spectrally-resolved (i.e., 1 nm resolution) full reflectance and fluorescence spectra for each pixel coordinate using a cubic spline interpolation, thereby generating a total of 723,840 spectra (696 x 520 =361,920 pixels x 2 exposures).

Tissue attenuation correction algorithm. The white light reflectance spectra corrected the detected fluorescence for the attenuation caused by tissue optical absorption and scattering[21]. Spectrally-constrained dual band normalization[26] was used to estimate the intrinsic fluorescence independently of the effects of tissue optical properties through the expression

$$\mathbf{\Phi}^{\mathbf{Fluo}}_{\mathrm{Corrected}}(\lambda) = \Omega \frac{\mathbf{\Phi}^{\mathbf{Fluo}}_{\mathrm{Raw}}(\lambda)}{\mathbf{\Phi}^{\mathbf{Ref}}_{\mathrm{x}} \times \left(\mathbf{\Phi}^{\mathbf{Ref}}_{\mathrm{m}}\right)^{\alpha}}$$

where $\Phi^{\mathbf{Fluo}}_{Raw}(\lambda)$ is the wavelength dependent, raw fluorescence intensity; $\Phi^{\mathbf{Ref}}_{\mathrm{x}}$ and $\Phi^{\mathbf{Ref}}_{\mathrm{m}}$ are the reflectance signals integrated over the ranges λ = 465−485 nm and λ = 625−645 nm, respectively; and Ω is a calibration factor that depends on the light source power. The range for $\Phi^{\mathbf{Ref}}_{\mathrm{x}}$ was selected to be close to the excitation wavelength band (i.e., 405 nm) to approximate light attenuation from excitation, whereas the range for $\Phi^{\mathbf{Ref}}_{\mathrm{m}}$ was chosen for the main emission peak of PpIX around λ = 635 nm. Our correction algorithm assumed that most of the light attenuation is due to absorption at the excitation wavelength, but scattering at the emission band can also be corrected with an empirical power function, α, of $\Phi^{\mathbf{Ref}}_{\mathrm{m}}$ (α = −0.7).

We applied this attenuation correction to each pair of reflectance and fluorescence image cubes. For each pixel coordinate (x_i, y_i), we integrated the reflectance spectrum to calculate $\Phi^{\mathbf{Ref}}_{\mathrm{x}}(\mathrm{i})$ and $\Phi^{\mathbf{Ref}}_{\mathrm{m}}(\mathrm{i})$, and estimated the corrected fluorescence, $\Phi^{\mathbf{Fluo}}_{Corrected}(\mathrm{i})$, at each pixel by normalizing its raw fluorescence spectrum, $\Phi^{\mathbf{Fluo}}_{Raw}(\mathrm{i})$ by these quantities. A least-squares estimate was applied to corrected fluorescence spectra to spectrally decompose the individual contributions of the main fluorophores: PpIX, fluorescein, and tissue autofluorescence through

$$\mathbf{C}^{rel} = \left(\mathbf{B}^T\mathbf{B}\right)^{-1}\mathbf{B}^T\Phi^{Fluo}_{Corrected}$$

where $\mathbf{B} = [\mathbf{b}_1\mathbf{b}_2\ldots\mathbf{b}_N]$ is a matrix of basis spectra for N fluorophore components (e.g., PpIX, fluorescein, autofluorescence), and $\mathbf{C}^{\mathrm{rel}}$ is a relative concentration fluorophore vector. A system-specific calibration factor, S_{cal}, derived from the least squares regression of phantom data of known PpIX concentrations converted the spectrally decomposed relative fluorophore concentrations into absolute concentrations for each pixel

$$\mathbf{C}^{abs} = S_{cal}\mathbf{C}^{rel}.$$

Tissue phantoms. Liquid phantoms that simulate brain tissue (and tumor) optical properties at the excitation and emission wavelengths were fabricated from a dye (McCormick) as the main absorber and Intralipid as the scattering medium. A total of nine (9) phantoms of three (3) different optical absorption ($\mu_{a,x}$ = 20, 40, and 60 cm^{-1}) and scattering values ($\mu'_{s,m}$ = 8.7, 11.4, and 14.5 cm^{-1}) were constructed (see **Table 1**). For each set of phantom optical properties, nine (9) PpIX concentrations covering the range found in brain tumors (0.019, 0.039, 0.078, 0.156, 0.313, 0.625, 1.250, 2.500, and 5.000 μg/ml) were added to produce a total of 81 phantoms of varying optical absorption, scattering and PpIX concentrations.

We acquired a pair of reflectance and fluorescence image cubes from each phantom under the low-light conditions typically found in the operating room during fluorescence-guided surgery. Each pair was processed with the spectrally-constrained normalization to form a PpIX concentration image. A region of interest corresponding to (x_i, y_i) pixel coordinates in the raw fluorescence image cube and in the calculated PpIX concentration image was identified for each phantom and used to (i) integrate the average area-under-the-curve intensity in the 610–720 nm range for the raw fluorescence spectra, $F_{\mathrm{RAW}} = \int_{610nm}^{720nm}\Phi^{\mathbf{Fluo}}_{Raw}(\lambda)d\lambda$), and (ii) construct the average PpIX concentration, C_{PpIX}, for the quantitative image map. The former represents the raw PpIX fluorescence, and is equivalent to using a bandpass filter to extract the signal in the range of interest. We also acquired images with the Zeiss Pentero surgical microscope adapted for visual fluorescence imaging (vFI). Briefly, fluorescence light in the range 450–720 nm was collected on a RGB CCD camera, and qualitative assessments of the level of visible fluorescence were made.

F_{RAW} and qFI-derived C_{PpIX} were obtained as a function of the true PpIX concentrations in each phantom. Linear regression was used to define the linearity in the fluorescence response with fluorophore concentration and the detection limits of both approaches.

Spectral decomposition of PpIX and fluorescein concentrations was evaluated with sixteen (16) additional phantoms at four different fluorescein concentrations (10, 5, 2.5, 1.25 μg/ml) and four PpIX concentrations (1.25,0. 625, 0.313, 0.156 μg/ml) with $\mu_{a,x}$ = 40 cm^{-1} and $\mu'_{s,m}$ =11.4 cm^{-1}. For each phantom, reflectance and fluorescence image cubes were acquired and our correction algorithm applied.

Animal studies. These studies were approved by the Institutional Animal Care and Use Committee (IACUC) at Dartmouth. Eight (8) Lewis rats were anesthetized by inhalation of isoflurane (2–4%) in 100% O_2. A 3 cm skin incision was made in the top of the cranium, a small bur hole drilled, and 5x10^5 CNS-1 tumor cells injected into the right striatum, and the wound closed using suture. The CNS-1 tumor cell line was chosen because it exhibits the histopathological hallmarks of human GBM, including invasion of parenchyma and periventricular spread with single cell infiltration[30].

Tumors were grown for two weeks, and on day 14 post-implantation, rats were given an i.p. dose of 100 mg/kg of ALA (Sigma) two hours prior to imaging. Animals were anesthetized for surgery by inhalation of isoflurane (2–4%) in 100% O_2 and a craniotomy performed, the dura removed, debris cleared, the brain exposed, and imaging performed. In 4 of the rats, an i.v. dose of 100 mg/kg of 10% fluorescein sodium solution in deionized water was administered post-dura opening.

Clinical studies. The Committee for the Protection of Human Subjects (CPHS), which governs the participation of humans in research at Dartmouth, approved our studies, and all patients participated under informed consent. Approximately 3 hours prior to the induction of anesthesia, patients were given an oral dose (20 mg/kg) of ALA (DUSA Pharmaceuticals, Tarrytown, NY, USA) dissolved in 100 ml of water.

At the discretion of the surgeon (DWR), the OM light was switched from white to blue exposure, and digital images of visible fluorescence, and reflectance and fluorescence image cubes were acquired. Coregistered probe measurements and biopsy specimens were collected with the latter immediately processed for subsequent histopathological analysis.

Histopathology. Histopathological analysis was performed on human formalin fixed paraffin embedded tissue and processed for H&E staining.

Data processing and analysis. Data processing and analysis were performed with MATLAB® software (Version R2010a, The Mathworks, Inc., Natick, MA, USA). Linear regression yielded the coefficient of determination, R^2. Paired Student's t-test was used to compare differences. Pearson's correlation coefficient was calculated to evaluate linearity between variables. Two-sided $P < 0.05$ was considered statistically significant.

1. Qiu, L. *et al.* Multispectral scanning during endoscopy guides biopsy of dysplasia in Barrett's esophagus. *Nat Med* **16**, 603–606, 601p following 606 (2010).
2. van Dam, G. M. *et al.* Intraoperative tumor-specific fluorescence imaging in ovarian cancer by folate receptor-alpha targeting: first in-human results. *Nat Med* **17**, 1315–1319 (2011).
3. Whitney, M. A. *et al.* Fluorescent peptides highlight peripheral nerves during surgery in mice. *Nat Biotechnol* **29**, 352–356 (2011).
4. Yoo, H. *et al.* Intra-arterial catheter for simultaneous microstructural and molecular imaging *in vivo*. *Nat Med* **17**, 1680–1684 (2011).
5. Sanai, N. & Berger, M. S. Glioma extent of resection and its impact on patient outcome. *Neurosurgery* **62**, 753–764; discussion 264–756 (2008).
6. Pouratian, N., Asthagiri, A., Jagannathan, J., Shaffrey, M. E. & Schiff, D. Surgery Insight: the role of surgery in the management of low-grade gliomas. *Nat Clin Pract Neurol* **3**, 628–639 (2007).
7. Smitt, M. C. *et al.* The importance of the lumpectomy surgical margin status in long-term results of breast conservation. *Cancer* **76**, 259–267 (1995).
8. Eastham, J. A. *et al.* Variations among individual surgeons in the rate of positive surgical margins in radical prostatectomy specimens. *The Journal of urology* **170**, 2292–2295 (2003).
9. Fisher, B. *et al.* Twenty-year follow-up of a randomized trial comparing total mastectomy, lumpectomy, and lumpectomy plus irradiation for the treatment of invasive breast cancer. *N Engl J Med* **347**, 1233–1241 (2002).
10. Karakiewicz, P. I. *et al.* Prognostic impact of positive surgical margins in surgically treated prostate cancer: multi-institutional assessment of 5831 patients. *Urology* **66**, 1245–1250 (2005).
11. Goharderakhshan, R. Z. *et al.* Utility of intraoperative frozen section analysis of surgical margins in region of neurovascular bundles at radical prostatectomy. *Urology* **59**, 709–714 (2002).
12. Jansen, M., Yip, S. & Louis, D. N. Molecular pathology in adult gliomas: diagnostic, prognostic, and predictive markers. *Lancet Neurol* **9**, 717–726 (2010).
13. Louis, D. N. *et al.* The 2007 WHO classification of tumours of the central nervous system. *Acta Neuropathol* **114**, 97–109 (2007).
14. Kriss, T. C. & Kriss, V. M. History of the operating microscope: from magnifying glass to microneurosurgery. *Neurosurgery* **42**, 899–907; discussion 907–898 (1998).
15. Willems, P. W., van der Sprenkel, J. W., Tulleken, C. A., Viergever, M. A. & Taphoorn, M. J. Neuronavigation and surgery of intracerebral tumours. *J Neurol* **253**, 1123–1136 (2006).
16. Galloway, R. L., Jr. The process and development of image-guided procedures. *Annu Rev Biomed Eng* **3**, 83–108 (2001).
17. Wen, P. Y. & Kesari, S. Malignant gliomas in adults. *N Engl J Med* **359**, 492–507 (2008).
18. Stummer, W. *et al.* Fluorescence-guided surgery with 5-aminolevulinic acid for resection of malignant glioma: a randomised controlled multicentre phase III trial. *Lancet Oncol* **7**, 392–401 (2006).
19. Pogue, B. W. *et al.* Review of Neurosurgical Fluorescence Imaging Methodologies. *IEEE J Sel Top Quantum Electron* **16**, 493–505 (2010).
20. Ntziachristos, V., Yoo, J. S. & van Dam, G. M. Current concepts and future perspectives on surgical optical imaging in cancer. *J Biomed Opt* **15**, 066024 (2010).
21. Bradley, R. S. & Thorniley, M. S. A review of attenuation correction techniques for tissue fluorescence. *J R Soc Interface* **3**, 1–13 (2006).
22. Valdes, P. A. *et al.* δ-aminolevulinic acid-induced protoporphyrin IX concentration correlates with histopathologic markers of malignancy in human gliomas: the need for quantitative fluorescence-guided resection to identify regions of increasing malignancy. *Neuro Oncol* **13**, 846–856 (2011).
23. Valdes, P. A. *et al.* Quantitative fluorescence in intracranial tumor: implications for ALA-induced PpIX as an intraoperative biomarker. *J Neurosurg* **115**, 11–17 (2011).
24. Richards-Kortum, R. & Sevick-Muraca, E. Quantitative optical spectroscopy for tissue diagnosis. *Annu Rev Phys Chem* **47**, 555–606 (1996).
25. Weissleder, R. & Pittet, M. J. Imaging in the era of molecular oncology. *Nature* **452**, 580–589 (2008).
26. Valdes, P. A. *et al.* A spectrally constrained dual-band normalization technique for protoporphyrin IX quantification in fluorescence-guided surgery. *Opt Lett* **37**, 1817–1819 (2012).
27. Kim, A., Khurana, M., Moriyama, Y. & Wilson, B. C. Quantification of *in vivo* fluorescence decoupled from the effects of tissue optical properties using fiber-optic spectroscopy measurements. *J Biomed Opt* **15**, 067006 (2010).
28. Tichauer, K. M. *et al.* In Vivo Quantification of Tumor Receptor Binding Potential with Dual-Reporter Molecular Imaging. *Mol Imaging Biol* (2011).
29. Ntziachristos, V. Going deeper than microscopy: the optical imaging frontier in biology. *Nature Methods* **7**, 603–614 (2010).
30. Jacobs, V. L., Valdes, P. A., Hickey, W. F. & De Leo, J. A. Current review of *in vivo* GBM rodent models: emphasis on the CNS-1 tumor model. *ASN Neuro* **3,** e00063 (2011).

Acknowledgements

This work was supported in part by National Institutes of Health grants R01NS052274-01A2 (DWR) and K25CA138578 (FL), as well as a Hitchcock Foundation Grant (PAV) and a Norris Cotton Cancer Multiple Investigator Prouty Grant (KDP, DWR, PAV). We acknowledge the support of Carl Zeiss (Carl Zeiss Surgical GmbH, Oberkochen, Germany) for use of the OPMI Pentero® operating microscope and DUSA Pharmaceuticals (DUSA Pharmaceuticals, Tarrytown, NY, USA) for their supplying of ALA. We thank R. Kinch for work with the custom optical adapter, K. Kolste for helpful discussions on system and algorithm design, and D. Valdes and Y. Wang for assistance with phantom experiments.

Author contributions

P.A.V., F.L., V.L.J., B.C.W., K.D.P., D.W.R. designed the experiments; P.A.V., F.L., B.C.W. designed the quantitative fluorescence imaging system. P.A.V. assembled the hardware and system software and performed the system performance and phantom studies. P.A.V., V.L.J. performed the pre-clinical rodent surgeries, imaging, and tissue studies. P.A.V., D.W.R. performed clinical data acquisition; D.W.R. performed the clinical surgeries. P.A.V. wrote the manuscript and performed the data analysis. P.A.V., K.D.P., D.W.R. supervised the project and manuscript preparation. All authors edited the manuscript.

Additional information

Supplementary information accompanies this paper at http://www.nature.com/scientificreports

Competing financial interests: The authors declare a US provisional patent application serial No. 61/588,708 on some aspects of the technology used in this study.

How to cite this article: Valdés, P.A. *et al.* Quantitative, spectrally-resolved intraoperative fluorescence imaging. *Sci. Rep.* **2**, 798; DOI:10.1038/srep00798 (2012).